Science of the Total Environment 635 (2018) 487–497

Contents lists available at ScienceDirect

Science of the Total Environment

journal homepage: www.elsevier.com/locate/scitotenv

Spatial-temporal change of land surface temperature across 285 cities in China: An urban-rural contrast perspective

Jian Peng [a], Jing Ma [a], Qianyuan Liu [b], Yanxu Liu [c], Yi'na Hu [a], Yingru Li [d], Yuemin Yue [e,*]

[a] Laboratory for Earth Surface Processes, Ministry of Education, College of Urban and Environmental Sciences, Peking University, Beijing 100871, China
[b] Key Laboratory for Environmental and Urban Sciences, School of Urban Planning and Design, Shenzhen Graduate School, Peking University, Shenzhen 518005, China
[c] State Key Laboratory of Earth Surface Processes and Resource Ecology, Faculty of Geographical Science, Beijing Normal University, Beijing 100875, China
[d] Department of Sociology, University of Central Florida, Orlando, FL 32816, USA
[e] Key Laboratory for Agro-ecological Processes in Subtropical Region, Institute of Subtropical Agriculture, Chinese Academy of Sciences, Changsha 410125, China

HIGHLIGHTS

- 98.9% of the cities in China showed UHI in summer nighttime.
- Most cities in China have higher increasing rate of nighttime LST in urban areas.
- Cities varied in LST characteristics have been classified into four types in China.
- The vital zone and major zone for UHI management are identified in China.

GRAPHICAL ABSTRACT

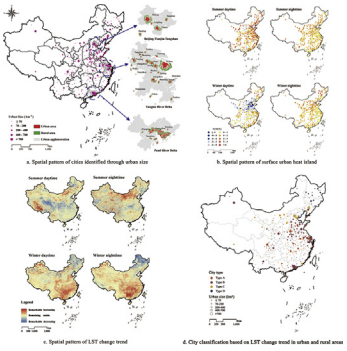

ARTICLE INFO

Article history:
Received 9 January 2018
Received in revised form 14 March 2018
Accepted 7 April 2018
Available online 24 April 2018

Editor: P. Kassomenos

Keywords:
Land surface temperature
Urban heat island
Cross-city comparison
City classification
Spatial-temporal change
China

ABSTRACT

As an important theme in global climate change and urban sustainable development, the changes of land surface temperature (LST) and surface urban heat island (SUHI) have been more and more focused by urban ecologists. This study used land-use data to identify the urban-rural areas in 285 cities in China and comparatively analyzed LST in urban-rural areas with the perspective of spatial-temporal dynamics heterogeneity. The results showed that, 98.9% of the cities exhibited SUHI effect in summer nighttime and the effect was stronger in northern cities than that in southern cities. In 2010, the mean SUHI intensity was the largest in summer daytime, with 4.6% of the cities having extreme SUHI of over 4 °C. From 2001 to 2010, the nighttime LST of most cities increased more quickly in urban areas compared with rural areas, with an increasing tendency of the urban-rural LST difference. The difference in the urban- rural LST change rate was concentrated in the range of 0–0.1 °C/year for 68.0% of cities in winter and 70.8% of cities in summer. For the higher LST increasing in urban areas compared with rural areas, there were more cities in summer than winter, indicating that the summer nighttime was the key temporal period for SUHI management. Based on the change slope of urban-rural LST, cities were clustered into four types and the vital and major zones for urban thermal environment management were identified in China. The vital zone included cities in Hunan, Hubei and other central rising provinces as well as the Beibu Gulf of Guangxi Province. The major zone included most of the cities in Central Plain Urban Agglomeration, Yangtze River Delta and Pearl River Delta. These results can provide scientific basis for SUHI adaptation in China.

* Corresponding author.
E-mail addresses: jianpeng@urban.pku.edu.cn (J. Peng), liuyanxu@pku.edu.cn (Y. Liu), yingru.li@ucf.edu (Y. Li), ymyue@isa.ac.cn (Y. Yue).

https://doi.org/10.1016/j.scitotenv.2018.04.105
0048-9697/

1. Introduction

Human activities have intense impacts on global material cycling and energy flow which gradually become an essential controlling factor in natural ecosystem (Zhou et al., 2016). City is the most concentrated area of human activities. The structure, function and dynamics of urban ecosystems have obvious human-induced characteristics (Xie et al., 2013), and the acceleration of urbanization has leaded to the reduction of species abundance, degradation of soil properties, changes in local climate and other negative ecological effects (Benz et al., 2017; Peng et al., 2016; Zhou et al., 2017a). The variation of the surface thermal environment is one of the important components of regional climate change.

The surface thermal environment is the manifestation of the heat exchange equilibrium between land and atmosphere, and it can be quantitatively described as land surface temperature (LST). As the result of the surface energy balance, LST is determined by local solar radiation, atmospheric properties, and surface properties (Kuang et al., 2015). During the process of rapid urbanization, impervious artificial surface, mainly construction land (Song et al., 2014), gradually replaces the natural and semi-natural surfaces, such as vegetation and water body, which originally exist in urban areas (Tran et al., 2017; Zhou et al., 2017b). This replacement changes the thermal environment of the urban surface, resulting in spatial difference in the energy exchange between the land and near-surface atmosphere (Liu et al., 2014; Weng et al., 2004; Yang et al., 2017). In addition, urban areas have more obvious surface thermal environment effect than rural areas, due to the anthropogenic heat discharge and the absorption, storage and reflection of solar radiation from urban buildings (Rizwan et al., 2008; Wang et al., 2015; Xie et al., 2013). The surface thermal environment effect generally manifests as the urban heat island (UHI) effect, which is a phenomenon that LST_u (urban land surface temperature) is higher than LST_r (rural land surface temperature) (Voogt and Oke, 2003). Many studies have shown that although UHI effect exists only as a local climate phenomenon, its impact on human health cannot be neglected (Merte, 2017; Zhao et al., 2014).

Quantitative monitoring and dynamic analysis of the UHI effect are the key contents of urban thermal environment research. Many scholars have agreed that UHI effect is increasing because of the intensifying urbanization (Chapman et al., 2017; Li et al., 2011; Mariani et al., 2016); thus, the seasonal and diurnal variation of UHI have long been key topics (Du et al., 2016; W. Zhou et al., 2014; D. Zhou et al., 2014). However, the conclusions drawn in previous studies are relatively inconsistent because of diverse quantification methods and various geographical locations, as well as the change of spatial range and other differences in the study areas. For example, Imhoff et al. (2010) found that the strongest UHI effect usually occurred in the daytime and summer in 38 most populated cities in USA. They also found that in summer daytime, the UHI intensity (7 to 9 °C) in regions that had densely planted vegetation such as temperate broadleaf and mixed forests was higher than that in the grassland vegetation region (4 to 6 °C), and the UHI effect in desert cities appeared to be weaker than in other cities. Hu and Brunsell (2013) studied the UHI in Houston, Texas, USA and the surrounding areas at six temporal scales, and found the UHI effect in spring and autumn was stronger than that in winter and summer. Schwarz et al. (2011) analyzed 11 quantitative indicators of UHI in 263 European cities, and found that most of the indicators leaded to the conclusion that the daytime UHI was stronger than the nighttime UHI, which was consistent with findings by Zhang et al. (2010). By monitoring the intensity of the meteorological heat island and the surface heat island in the Beijing-Tianjin-Hebei region of China in July, Wang et al. (2016) found that for both air UHI and surface UHI, the intensity of the nighttime heat island was much higher than that in the daytime, being the greatest (4–6 K) at 04:00 and the smallest (1−2 K) at 12:00 (noon), respectively. However, Zhao et al. (2014) pointed out that cities in humid regions experienced higher daytime annual-mean UHI intensity than cities in dry regions. Therefore, the universal law of diurnal and seasonal variation of the UHI effect under different ecological backgrounds needs further exploration and summarization.

As one of the fastest urbanizing countries in the past 30 years, China's urbanization rate is 2.14% faster than the world average, with urban areas growing by an average of 7.9% per year (Seto et al., 2011). China's urban population has increased from 170 million to 730 million since the implementation of the reform and opening up policy; and China may continue to be the world's fastest growing country in the next 50 years or more (Kuang et al., 2016; Seto et al., 2012). Accordingly, the thermal environment effect especially UHI effect in China is relatively more typical and apparent in contrast to other regions or countries (Zhou et al., 2004). In 2014, China's National New-type Urbanization Plan (2014–2020) set ecological civilization and green low carbon as one of the vital principles to guide national urbanization and social development for the next 15 years. Thus, questions about how to develop in a low-carbon way, manage greenhouse gas emission effectively and enhance the adaptability to UHI, become scientific subjects for scholars from different fields as well as the crucial social issues that affect the daily lives of urban residents in China.

Previous UHI studies in China mainly focused on a certain city or urban agglomerations, with the following key areas: (1) mega-urban agglomerations (Du et al., 2016; Liu et al., 2017; Wang et al., 2016); (2) the megalopolis (Li et al., 2011; Peng et al., 2016); (3) booming cities (Dan et al., 2011; Yu et al., 2018); and (4) furnace cities (Shen et al., 2016; Shi et al., 2012; Yao et al., 2015). There were few studies conducted at the national scale (D. Zhou et al., 2014; Yao et al., 2017), and even in these studies it was typical kind of cities that were focused. There is a lack of comprehensive understanding among cities of different sizes in various climate zones, which needs further spatial-temporal comparison analysis. Therefore, this study examined 285 cities at prefecture-level or above in mainland China and analyzed the spatial heterogeneity of LST in urban and rural areas, as well as the change tendency. The objectives of the study were to: (1) identify spatial pattern of urban and rural areas of cities in mainland China based on the land-use data using a city clustering algorithm and buffer analysis; (2) using linear regression, analyze the change tendency of UHI based on the winter-summer and diurnal change rate of LST_u and LST_r; and (3) classify the 285 cities into four types using K-means clustering based on the change of LST_u and LST_r.

2. Methodology

2.1. Study area

In essence, the entirety of mainland China was selected as the study area, although only 285 cities at prefecture-level or above were examined. China has a vast territory and abundant resources, various geological and hydrothermal conditions have inevitably resulted in diverse soil, hydrological and vegetation conditions. The average temperature in the eastern half of the country decreases from the south to the north. In the western part, the annual mean temperature in the southern Qinghai-Tibet Plateau is generally below 0 °C, but it is above 5 °C in the northern Tarim Basin. The precipitation decreases from the southeast coast to the northwest inland, and tends to decrease rapidly from coastal areas to inland areas.

Affected by natural resources, the social and economic development in China present remarkable diversity. The urbanization in China has rapidly developed from a starting point as a result of accelerating industrialization since the implementation of the reform and opening up policy. According to China's National New-type Urbanization Plan (2014–2020), the population urbanization rate had increased from 17.9% to 53.7%, and the number of cities had increased from 193 to 658 during the urbanization process by 2013 (Song and Deng, 2015), with the Pearl River Delta (PRD), Yangtze River Delta (YRD) and Beijing-Tianjin-Hebei (BTH) urban agglomerations gradually formed.

Economic growth has inevitably caused the spatial agglomeration of population and industrial activities. The average size of cities has been increasing, and small towns have developed rapidly as well. According to the universal law of global urbanization, China is still experiencing the rapid development stage in which the urbanization rate is 30–70%. As a result, urbanization will be the main social development process that characterizes China throughout the near future.

In China, the stage and characteristics of urbanization of each city are different because of the differences in regional natural conditions, industrial structure, economic systems, and regional development strategy and policy. Generally speaking, cities with >5 million residents are mostly distributed in the coastal areas, as are more than half of the cities with 1–2 million inhabitants. Cities with populations of 2–5 million and under 200,000 residents are evenly distributed throughout the country. As a result, regional differences of natural ecosystems and social economics are significant, making China an ideal study area for exploring urbanization and its eco-environmental effects.

2.2. Urban-rural areas identification

City is defined broadly as a permanent large settlement compared with the countryside, but this definition is an abstract concept without spatial identification. Using the City Clustering Algorithm (CCA) (Peng et al., 2012; Rozenfeld et al., 2008) and buffer analysis (Imhoff et al., 2010), this study conducted the identification of urban and rural areas of 285 cities in mainland China by using the land-use data.

To identify the urban and rural areas, the consecutive artificial surface pixels surrounding the city administrative center were defined as built-up area or urban area based on the breadth of the priority search in the CCA. Next, two buffers from the urban area to the outside were created to identify the corresponding rural area (Fig. 1). Using concentrated urban construction area to represent the actual urban area and thus determine the rural area based on the urban size, this procedure had the advantage of transcending administrative divisions. The identification of urban and rural areas was made according to the following rules:

a. If the urban areas of several cities are spatially connected, the cities are regarded as one city.
b. For cities in which rivers or mountains go through the urban area (i.e., multi-core cities), the administrative center of districts or towns is added to ensure the urban areas can be identified completely.
c. The construction land will be excluded if it is disconnected with the urban area where the municipality is located due to non-natural reasons (e.g. rivers, mountains).
d. The first buffer of the urban area is regarded as the corresponding urban fringe.
e. The second buffer (without construction land and water pixels) of the urban area is regarded as the corresponding rural area.

The GlobeLand30 dataset (30-m resolution) for 2010 was obtained from the National Basic Geographic Information Center (www.globallandcover.com) and was used as the basic layer for identifying urban and rural areas. The dataset is the global surface coverage data based on Landsat TM and ETM+ images, incorporating Chinese Environmental Disaster Alleviation Satellite (HJ-1) and the Beijing No. 1 small satellite (BJ-1) data with the MODIS NDVI data through phonological information mining and seasonal phase difference correction. The dataset identifies water body, wetland, artificial surface, tundra, permanent snow and ice, grassland, barren land, cultivated land, shrub land and forest land, with the overall classification accuracy of 80% (Chen et al., 2014). Combined with data from the China Statistical Yearbook of 2011 and the city administrative center location data from China's 1:4 million basic geography dataset, the locations of 287 cities at prefecture-level or above in mainland China for the year 2010 were extracted. Then the urban area, fringe area and rural area of each city were spatially identified.

2.3. LST linear regression

Monthly LST during 2001–2010 from the MODIS dataset (MODLT1M) was used, which was a synthetic product of the mean monthly value of MODLT1T provided by the International Scientific & Technical Data Mirror Site, Computer Network Information Center and Chinese Academy of Sciences (http://www.gscloud.cn). By using these data, the annual change tendency was quantified in the view of diurnal and seasonal contrast, with spatial pattern analysis of LST in China.

First of all, the Maximum Value Composite (MVC) method was used to determine the diurnal LST in winter (December–February) and summer (June–August) of each year during 2001–2010. Given the geographic conditions of China and the research purpose, only the data in June–August and December–February were used to represent the summer and winter LST and UHI, with the spring and autumn UHI excluded. Any missing values were amended using the mean value of each series. Then, four time-series for 2001–2010 were built that included summer daytime LST, winter daytime LST, summer nighttime LST and winter nighttime LST. Winter and summer LST are mostly considered in the study on climatic response to urbanization, particularly on seasonal variation in thermal environment response (Peng et al., 2012; Schwarz et al., 2011; Zhou et al., 2004). Since the seasonal difference of heat and moisture reached the largest between winter and summer, both seasons were taken into account for the study on seasonal variation of thermal environment. Thirdly, the seasonal and diurnal mean values for LST_u and LST_r of each city for pixels were calculated using the results of the urban and rural area identification and MODLT1M data for

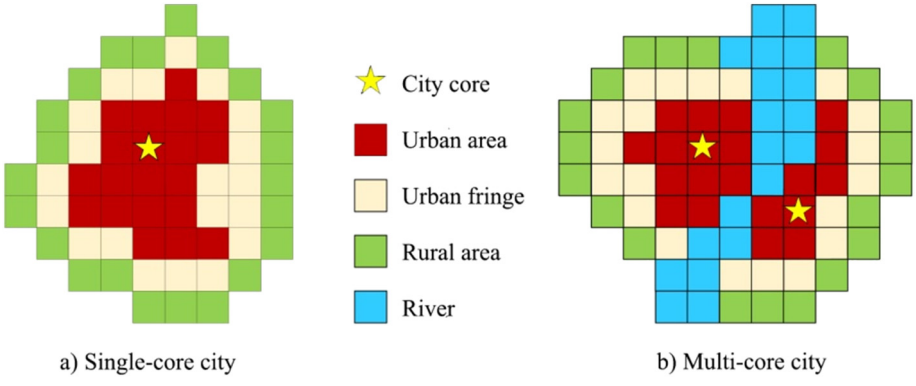

Fig. 1. Graphical representation of urban-rural areas identification.

2001–2010. ΔLST was then calculated as the difference between LST_u and LST_r to quantify the surface urban heat island (SUHI) of each city.

In the final step, the four sets of time-series data were composited into a 10-band multiband image and the *Slope* of LST change was measured using pixel-by-pixel linear regression analysis. Then Δ*Slope* was defined as the difference between the *Slope* for LST_u and LST_r, as described by Eq. (1).

$$Slope = \frac{n \times \sum_{t=1}^{n} t \times LST_t - \left(\sum_{t=1}^{n} t\right)\left(\sum_{t=1}^{n} LST_t\right)}{n \times \sum_{t=1}^{n} t^2 - \left(\sum_{t=1}^{n} t\right)^2} \quad (1)$$

In Eq. (1), n is the length of time series in years ($n = 10$), t is the time point ($t = 1, 2, \ldots, 10$), and LST_t is the LST of a pixel at time t. If the value for *Slope* is positive, it denotes an increasing tendency in LST; conversely, a negative value for *Slope* indicates a cooling tendency. The larger is the absolute value of *Slope*, the larger is the variation rate of LST. The significance of regression relationship was set to the level of 0.05.

To analyze the LST change tendency, spatial pattern of LST variation was comparatively analyzed according to the absolute value of *Slope* (the variation rate of LST), and the mean *Slope* of each city's urban and rural area was calculated using the tool of Zonal Statistics as Tables in ArcGIS 10.2 (ESRI Inc., Redlands, CA, USA) to get the range/amplitude [Minimum, Maximum] of *Slope*.

2.4. K-means clustering

K-means clustering usually partition n observations into K clusters ($K \ll n$), making the difference among samples in each cluster as small as possible so that clusters can be identified effectively. In this study, K points were randomly selected as centroids in the samples, which roughly divided the samples into K clusters. Then, the distance from all sample points to these centroids was calculated and thus each sample point could be classified into the nearest cluster to replace the primary classification. Furthermore, the average value of the grouped points was set as the new centroid and the reclassification was conducted. Finally, whether the result was reasonable was examined and, if not, the classification schemes would be adjusted by the distance from the centroids until the convergence was reached.

In short, the city classification was conducted using eight indicators, including the *Slope* of LST change for each city's urban and rural area in summer daytime, summer nighttime, winter daytime and winter nighttime based on the K-means clustering (Chen et al., 2017; Nishiyama et al., 2007; Walelign, 2016).

3. Results and discussion

3.1. Spatial pattern of cities with different sizes

Most of the cities focused in this study are located in eastern China. It's obvious that the BTH, YRD and PRD urban agglomerations have greatly larger urban size than other regions. The urban areas of Foshan City and Guangzhou City in Guangdong Province are adjacent in space as well as Xi'an City and Xianyang City in Shaanxi Province, and these spatially connected cities were defined as urban consortium in this study. Cities belong to the same urban consortium have closer interaction and more frequent communication with each other, with similar natural conditions. The eco-environmental problems brought about by

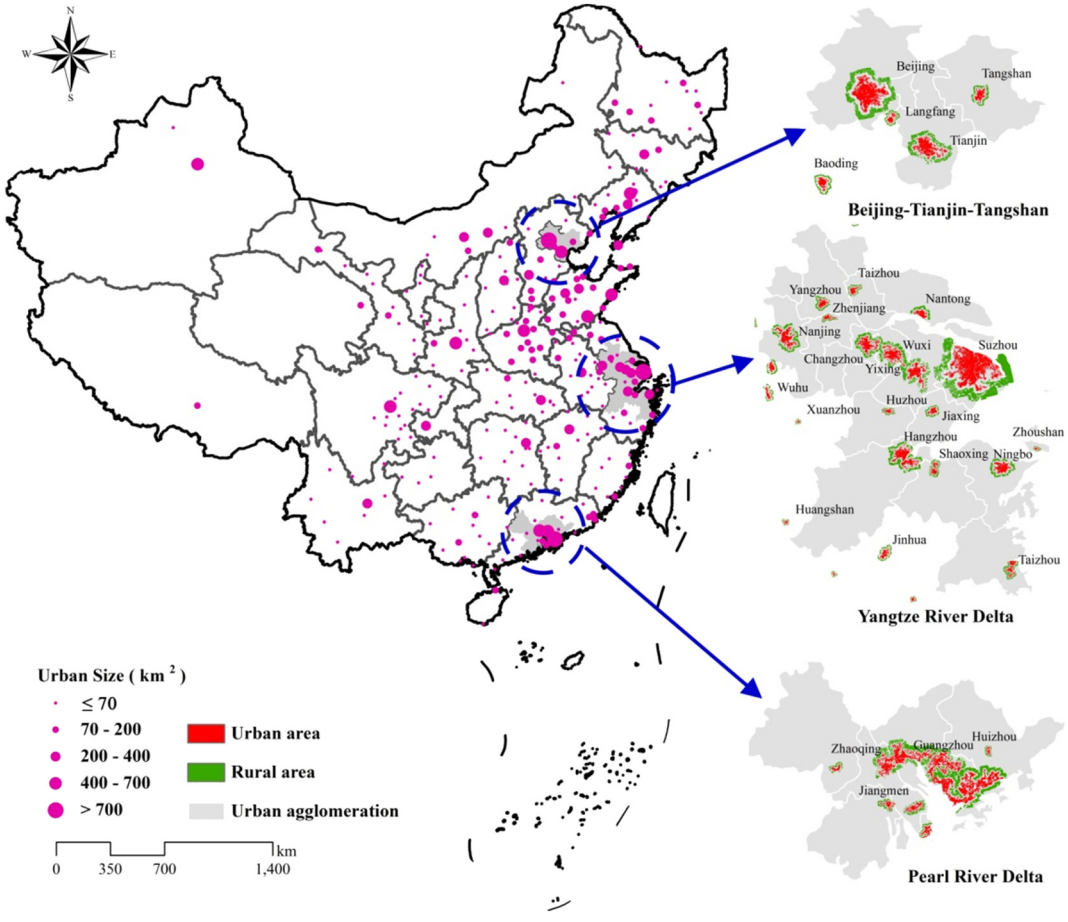

Fig. 2. Spatial pattern of cities identified through urban size.

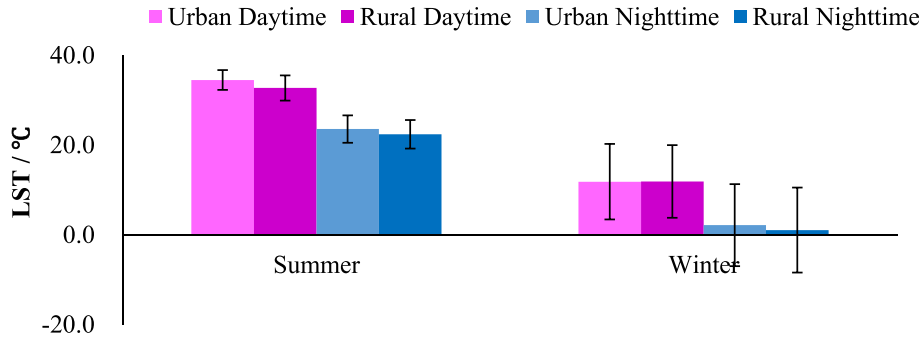

Fig. 3. Mean land surface temperature (LST) of urban and rural areas in summer and winter during 2001–2010.

urbanization have a high degree of symbiosis and spatial consistency within these regions.

As a result, 287 cities were originally identified, and then condensed into 285 cities or city consortiums through the urban-rural areas identification (Fig. 2). The size of these urban areas was divided into five classes using the natural break method. There were 62.8% of cities with an area <70 km^2, with 25.3% of cities having an area of 70–200 km^2. These relatively small size cities were mainly distributed in western provinces such as Yunnan, Guizhou, Gansu, Ningxia, Qinghai, and Tibet. Only 11.9% of cities had an area larger than 200 km^2; 21 of these covered 200–400 km^2 and were mostly distributed in the eastern China. Cities with an area in the range of 400–700 km^2 included Urumchi, Qingdao, Dongguan, Zhengzhou, Chengdu, Linyi, Tianjin, Shenyang, Xi'an-Xianyang and Guangzhou-Foshan. Cities with an area exceeding 700 km^2 included only Beijing, Shenzhen and Shanghai, and the urban sizes of them all exceeded 1000 km^2. In accordance with the pyramid rule of urban size, the larger is the urban size, the higher is the city level, and the fewer are the total number of cities at that level.

3.2. Seasonal and diurnal contrast of urban-rural LST

The mean seasonal and diurnal LST_u and LST_r of all the cities in the period 2001–2010 were counted and comparatively analyzed to characterize the national surface thermal environment (Fig. 3). It could be found that the mean LST in urban areas was higher than that in rural areas whenever it was daytime or nighttime in winter or summer, indicating the occurrence of UHI effect. As shown in Fig. 3, the difference of mean LST between urban and rural areas, ΔLST in summer was greater than that in winter. In summer, the daytime ΔLST (1.79 °C) was larger than the nighttime ΔLST (1.17 °C), while in winter, the daytime ΔLST (0.05 °C) was smaller than the nighttime ΔLST (1.09 °C). The seasonal and diurnal characteristics of ΔLST were consistent with the results of D. Zhou et al. (2014).

The standard deviations of LST (LST-Std) in each city's urban areas (LST_u-Std) and rural areas (LST_r-Std) were also calculated to evaluate the degree of dispersion in LST. In summer, the LST-Std of urban daytime, rural daytime, urban nighttime, rural nighttime was 2.21, 2.81, 3.05 and 3.18, while in winter, the comparable LST-Std was 8.42, 8.10, 9.14 and 9.47, respectively. In general, the LST-Std in summer was smaller than that in winter, the LST-Std in the daytime was smaller than that in the nighttime, and the LST-Std in urban areas was smaller than that in rural areas.

In summer, the LST difference between cities in tropical and temperate areas is low as a result of the sun irradiating the Tropic of Cancer directly. However, the LST of cities in central and northern areas will decrease significantly in winter because the sun irradiates the Tropic of Capricorn directly, while the LST of cities in tropical and subtropical areas remains stable, resulting in increasing ΔLST among the cities. For the diurnal contrast, the whole study area is irradiated by the sun in the daytime, and the combined impacts of surface attributes and the land's specific heat capacity will decrease the differences between LST in the dry cold areas and the humid coastal areas. The diurnal temperature difference in the arid areas is larger than that in the moist areas. Hence, the dispersion degree of LST in the nighttime is larger than that in the daytime. The reason why LST_u-Std was smaller than LST_r-Std is probably because the urban thermal environment is mainly influenced by human activities and anthropogenic heat discharge (Wang et al., 2015). These artificial factors can strongly affect the natural environment in urban areas such as similar changes of land cover and land use (Tran et al., 2017). In contrast, in rural areas the vegetation conditions and surface attributes remain mostly natural, showing a distinctive regional heterogeneity.

China is a vast country with many climate zones, diverse geographical and climatic conditions in each city resulting in different thermal environment characteristics. To further explore the differences between the urban and rural thermal environment, ΔLST was used to represent SUHI (Li et al., 2017). The SUHI in summer daytime (SUHI_SD), summer nighttime (SUHI_SN), winter daytime (SUHI_WD) and winter nighttime (SUHI_WN) of each city was calculated using the LST in 2010, respectively. The SUHI range was divided into 10 classes at an interval of 1 °C, and the values of SUHI >0 referred to a heat island, with values of SUHI <0 for a cold island.

The results showed that most cities experienced UHI effect regardless of the seasonal or diurnal variation (Fig. 4). A higher proportion of cities had greater LST_u than LST_r at night (98.9% in summer and 94.4% in winter) than during the daytime (88.8% and 56.8% in summer and winter, respectively). The total area of cities that experienced the UHI effect was maximal in the nighttime of summer. The UHI effect varied between seasons and between day and night. According to the

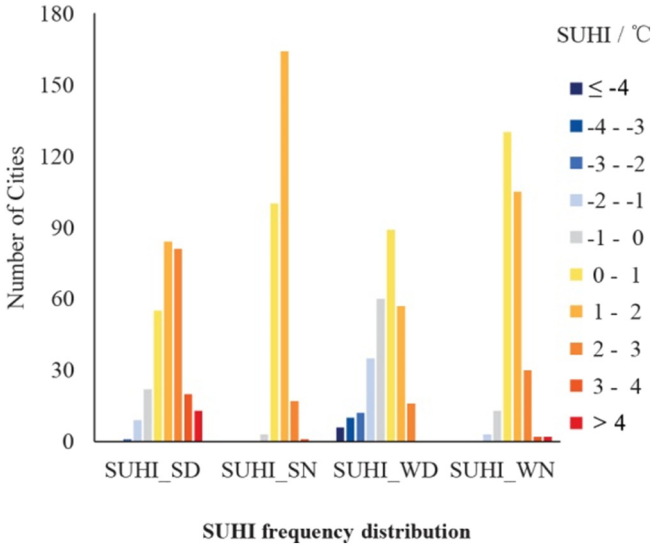

Fig. 4. Frequency distribution of surface urban heat island (SUHI) in summer daytime (SD), summer nighttime (SN), winter daytime (WD) and winter nighttime (WN).

differences among the mean and standard deviation of ΔLST of all cities in four temporal periods, i.e. SUHI_SD (1.61 ± 1.35 °C), SUHI_SN (1.19 ± 0.52 °C), SUHI_WN (1.06 ± 0.78 °C), and SUHI_WD (0.01 ± 1.54 °C), which were statistically significant ($P < 0.05$), the SUHI effect was the strongest in the daytime of summer. Furthermore, in summer daytime, 40.0% of the cities had SUHI over 2 °C and 4.6% of the cities appeared to have extreme SUHI over 4 °C (Fig. 4).

The SUHI also exhibited significantly spatial heterogeneity (Fig. 5). In southern China, higher soil moisture leaded to lower nighttime cooling amplitude in rural areas, which resulted in weaker nighttime SUHI compared with the northern China (Yao et al., 2017; D. Zhou et al., 2014). As the manifestation of the difference of energy stored in the daytime between urban and rural areas, the nighttime SUHI was mostly affected by the scale and intensity of human activities rather than seasons. Thus, spatial distribution of nighttime SUHI was similar in winter and summer. However, spatial pattern of daytime SUHI was relatively different because of the seasonal variation of solar radiation during the daytime. In the daytime, there were usually more cities with severe hot islands in summer and severe cold islands in winter.

3.3. LST change tendency

The LST change trend based on linear regression analysis (Fig. 6) showed that the spatial pattern of *Slope* (the change trend of LST) was not completely consistent between daytime and nighttime or between winter and summer. The difference in *Slope* between daytime and nighttime was much smaller than that between winter and summer in general, which indicated that the factor determining the spatial pattern of LST change was seasonally varied. From the perspective of seasonal differentiation, the warming (LST-increasing) areas in summer were not as concentrated as those in winter. The warming areas in winter were mainly distributed in the southeast of China with flatlands and

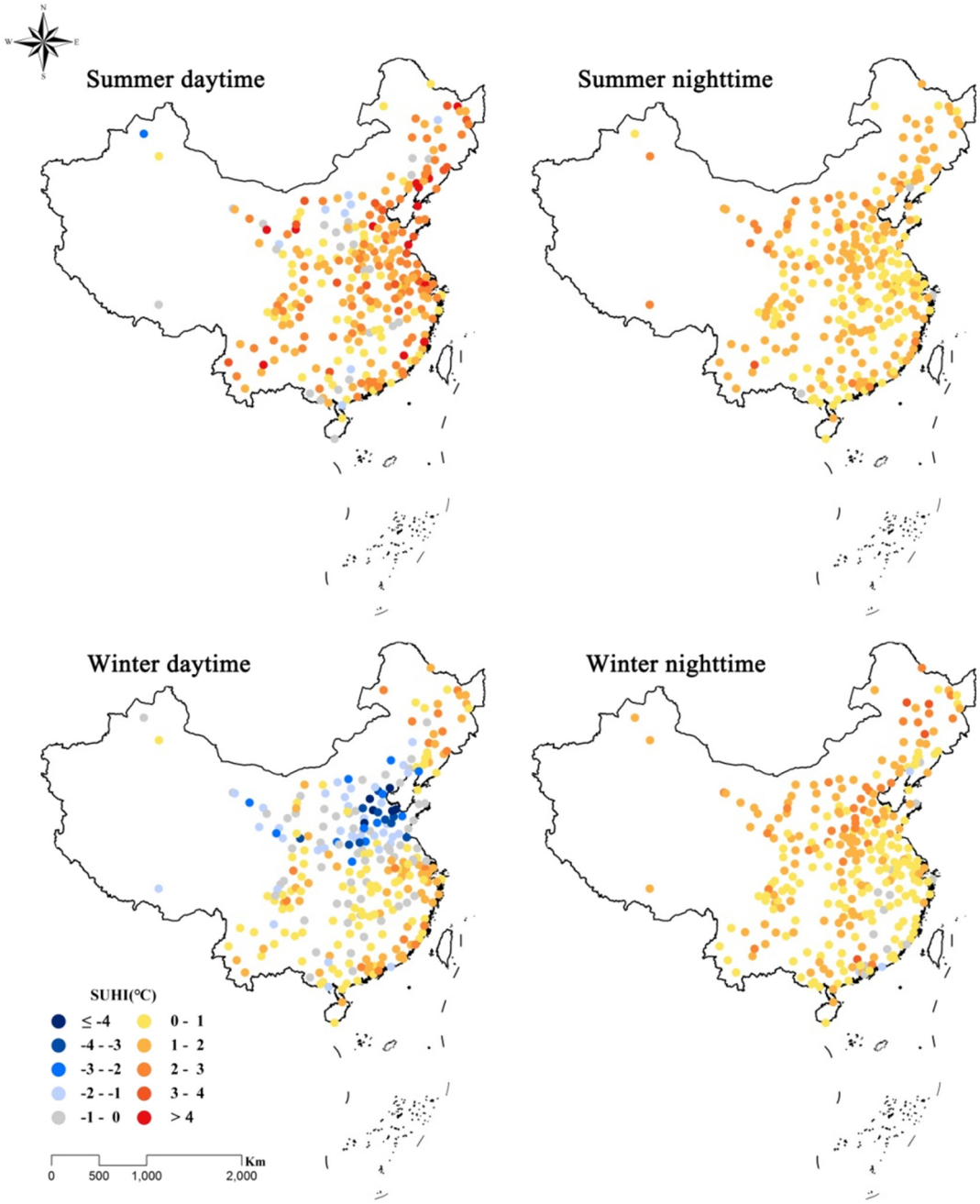

Fig. 5. Spatial pattern of surface urban heat island (SUHI) in China's 285 cities in 2010.

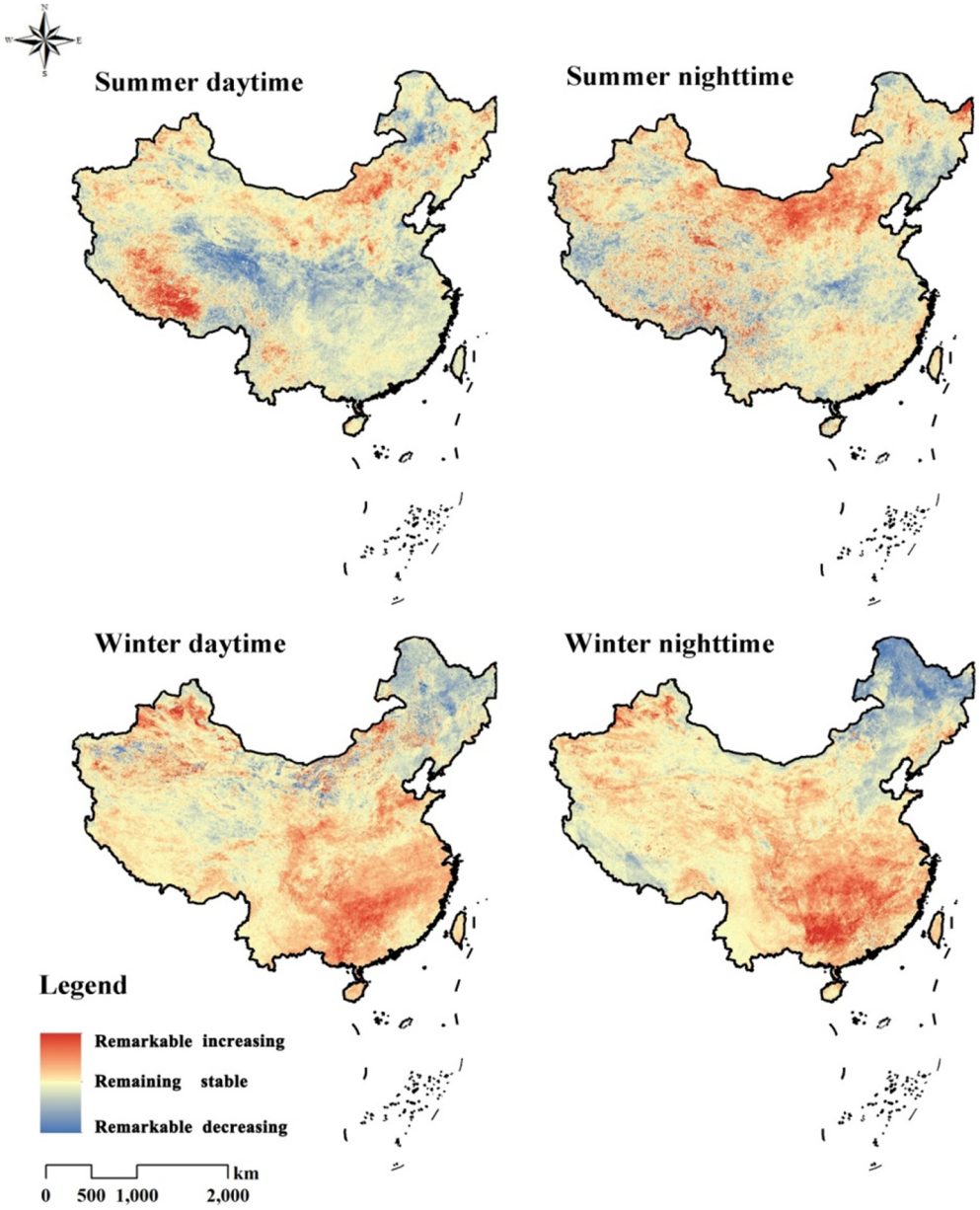

Fig. 6. Spatial patterns of change trend of land surface temperature (LST) during 2001–2010.

well-developed cities. The warming areas in summer exhibited a contrary spatial pattern and were mainly distributed in arid and semi-arid parts of northern China such as part of Inner Mongolia Plateau and Qinghai-Tibetan Plateau, which had higher *Slope* values than the southeastern areas. In addition, in terms of diurnal differentiation, spatial patterns of positive *Slope* in daytime and nighttime were similar in the same season. The total LST-increasing zone was larger at night than in the daytime, with more scattered spatial distribution.

The range of *Slope* and other descriptive statistics were shown in Table 1. In the daytime, the range of $Slope_r$ (*Slope* of the rural areas) was greater than $Slope_u$ (*Slope* of the urban areas), whether it was in summer or winter. However, in the nighttime, the difference between the range of *Slope* for rural and urban areas was negligible both in summer and winter. It could be concluded that, $Slope_u$ was more spatially consistent than $Slope_r$, indicating that the driving factors of urban LST change might be similar in different cities when excluding the seasonal

Table 1
Statistics of surface urban heat island (SUHI) in 2010 and the change trend of land surface temperature (LST) during 2001–2010 among China's 285 cities.

Temporal period	SUHI (°C)	Urban LST change slope (°C/year)		Rural LST change slope (°C/year)	
	Mean ± Std.	Mean ± Std.	Minimum, maximum	Mean ± Std.	Minimum, maximum
Summer daytime (SD)	1.61 ± 1.35	0.02 ± 0.16	−0.43, 0.80	0.04 ± 0.18	−0.58, 1.00
Summer nighttime (SN)	1.19 ± 0.52	0.03 ± 0.09	−0.15, 0.35	0.02 ± 0.08	−0.18, 0.31
Winter daytime (WD)	0.01 ± 1.54	0.07 ± 0.26	−0.72, 0.89	0.10 ± 0.28	−0.83, 0.92
Winter nighttime (WN)	1.06 ± 0.78	0.11 ± 0.21	−0.65, 0.67	0.09 ± 0.21	−0.62, 0.67

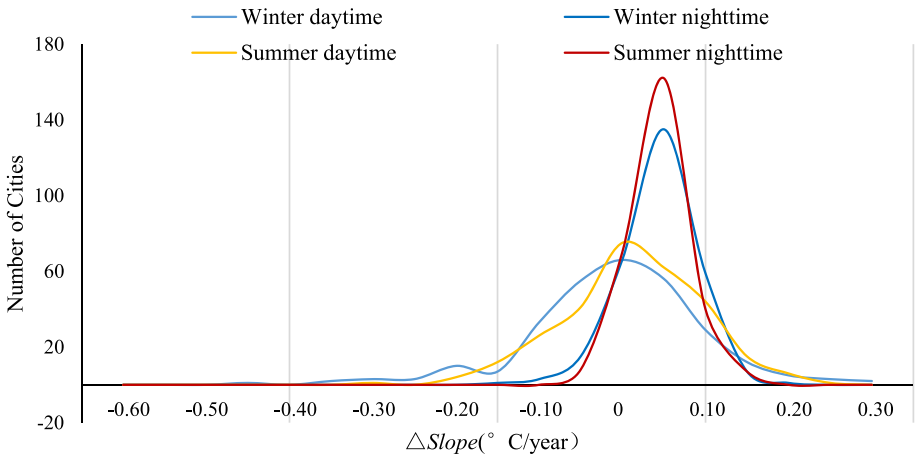

Fig. 7. Frequency distribution of Δ*Slope* between urban and rural areas.

and diurnal impacts. It could also be found that the individual values for $Slope_u$ and $Slope_r$ were both in accordance with *Slope* for the whole city, indicating that the *Slope* was dominated by geographical location which referred to the combination of various natural conditions.

Furthermore, the frequency distributions of Δ*Slope* were mapped (Fig. 7) and discussed in the view of contrast. Firstly, it came to diurnal contrast. In the daytime, the frequency distribution of Δ*Slope* was symmetrically distributed around 0 °C/year, especially in the winter daytime. The total number of cities that exhibited positive Δ*Slope* was almost equal to the number of cities with negative Δ*Slope* during 2001–2010. However, the frequency distributions of Δ*Slope* were symmetrically distributed around 0.05 °C/year for the nighttime period, which meant there were more cities with faster increasing of LST_u than LST_r. As a result, there was an increasing trend of ΔLST in the nighttime. Furthermore, the frequency distribution curves of Δ*Slope* in the daytime were flatter than that in the nighttime, and the nighttime curves had more prominent peaks, indicating that the daytime Δ*Slope* was distributed more homogeneously than the nighttime one. As shown in Fig. 7, in the nighttime, 68.0% of the cities in winter with 70.8% for summer had a Δ*Slope* in the range of 0–0.10 °C/year, indicating again the increasing trend of nighttime ΔLST. Secondly, it came to seasonal contrast. The frequency distribution curve of Δ*Slope* in winter was flatter than that in summer, which meant the winter Δ*Slope* of cities was more widely dispersed than the summer one. In addition, the symmetry axis of the frequency curve in summer was slightly shifted to the right compared with that in winter. This indicated that the $Slope_u$ in summer was obviously larger than that in winter and there were more cities exhibiting this phenomenon. As a result, the urban warming tendency was more apparent than the rural one. In summary, summer nighttime should be more focused for LST change monitoring and SUHI assessing.

3.4. City classification based on LST change trend

Based on LST change in urban and rural areas, 285 cities were divided into four types (designated as A, B, C and D) using the K-means clustering procedure in IBM SPSS Version 20.0 (IBM Corp., Armonk, N.Y., USA) (Fig. 8, Table 2). Generally speaking, LST_u increased more slowly in the daytime but faster at night than LST_r when LST was increasing, indicating that ΔLST would decrease in the daytime and increase in the nighttime. Because the diurnal LSTs in the urban and rural areas increased at different rates, there was an increasing tendency of SUHI effect in the nighttime. Furthermore, considering that the Δ*Slope* could substantially indicate the change trend of SUHI effect, the major zones and key temporal periods for urban thermal environment management were identified through LST change analysis.

Cities classified as Type A (N = 75) had increasing LST both in summer and winter, with a nighttime SUHI. In Type A cities, LST increased severely over the entire study period (2001−2010) with faster increasing rate in winter than in summer and in the daytime than in the nighttime. Compared with LST_r, the LST_u increased more rapidly in the nighttime but more slowly in the daytime. As a result, the nighttime SUHI tended to continuously exacerbate. Located in the north of PRD urban agglomeration and the west of YRD urban agglomeration, Type A cities were mainly distributed in the provinces of Hubei, Hunan, Jiangxi and Anhui as well as the Beibu Gulf Economic Rim in Guangxi Province, which was one of the national key developing areas in the 13th Five-Year Plan. Located in the radiating areas of the two urban agglomerations with national preferential urbanization policy, Type A cities experienced remarkable socio-economic development. In conclusion, as the forerunner area of national strategy of urbanization, type A cities located in the most actively urbanizing regions, with the nighttime SUHI effect continuously exacerbating under the condition of the whole LST increasing. Therefore, they should be designated as the vital zone for managing urban thermal environment, especially for the nighttime SUHI adaptation in China.

Type B cities (N = 133) experienced LST increasing in winter and a nighttime SUHI. These cities showed a slightly cooling tendency in summer daytime but a strongly warming tendency at other times, and LST_u increased faster than LST_r in the nighttime. Type B cities were mainly distributed in the Central Plain Urban Agglomeration, as well as in the YRD, PRD and other southeastern coastal areas. These cities were characterized by large urban size and high-level urbanization stage, and would continue to be the core area of China's urbanization in the near future. In correspondence with Type A cities, the nighttime SUHI tended to be exacerbated with a high increasing speed. Hence, Type B cities should be designated as the major zone for urban thermal environment management.

Type C cities (N = 45) experienced LST increasing in summer and a nighttime SUHI. These cities exhibited a slightly cooling tendency in winter daytime but a remarkably warming tendency in summer, and in the nighttime LST_u increased faster than LST_r. Hence, the nighttime SUHI (especially in summer) was expected to exacerbate in the future. These cities were centrally situated in the arid and semi-arid area of northwestern China. In addition to the cities in the provinces of Gansu and Ningxia, which had small urban size because of the restricted natural resources, other cities in Type C were generally large such as Beijing, Tianjin and other megalopolises, as well as other big cities in Inner Mongolia and Shaanxi Province with rich natural resources. Cities in Type C had a high and increasing occurrence rate of the nighttime SUHI, especially in summer. In the future, SUHI effect of Type C cities should be alleviated by controlling the intensity of human activities

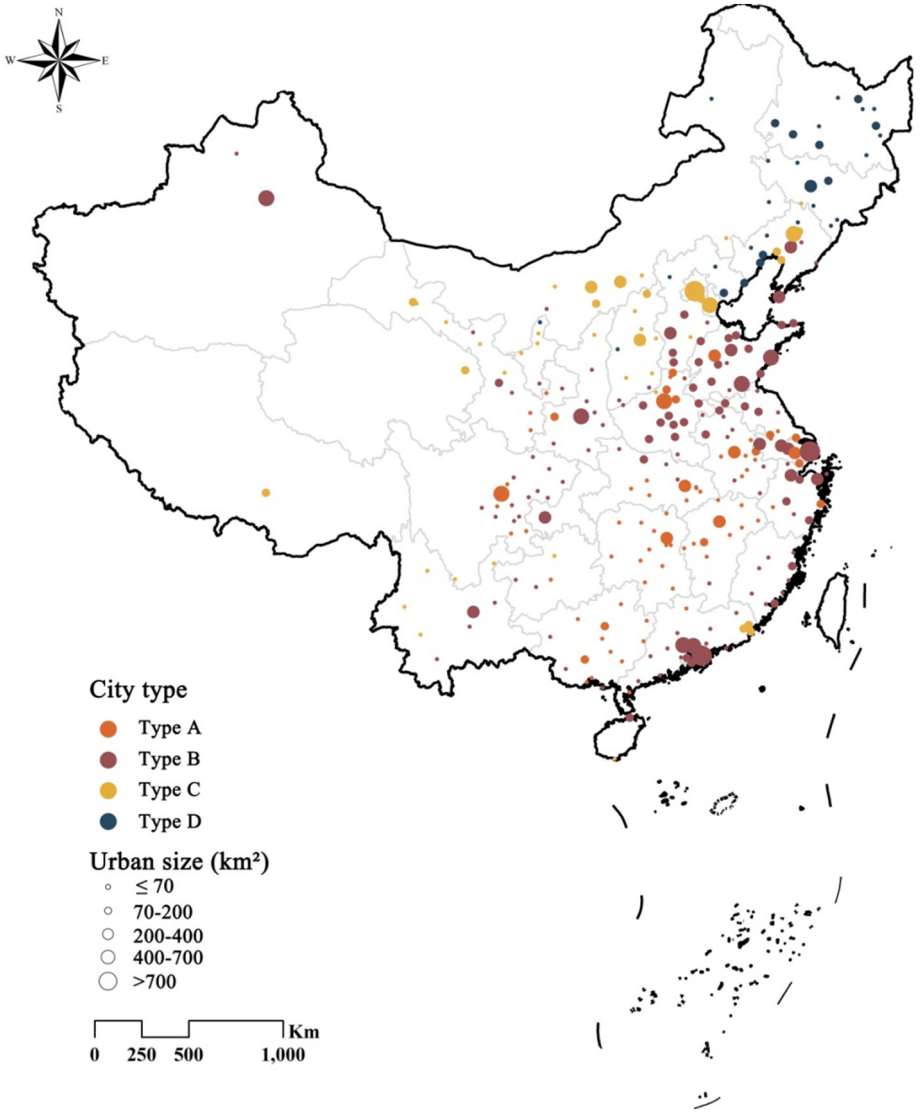

Fig. 8. City classification based on land surface temperature (LST) change trend in each city's urban and rural areas (Type A, cities with increasing LST in summer and winter, and a nighttime SUHI; Type B, cities with increasing LST in winter and a nighttime SUHI; Type C, cities with increasing LST in summer and a nighttime SUHI; and Type D, cities with increasing LST in summer and decreasing LST in winter).

and anthropogenic heat emissions (Mohajerani et al., 2017). Moreover, the vegetation coverage in Type C cities could be improved through enhancing urban tree canopy (Elmes et al., 2017) because the photosynthesis and transpiration of the plant communities would help to SUHI alleviation (Gunawardena et al., 2017; Shiflett et al., 2017; Zhou et al., 2017b).

Type D cities (N = 32) experienced LST increasing in summer and LST decreasing in winter. These cities were intensively located in the northeast of China. The LST had a slightly increasing tendency in summer and a clearly decreasing tendency in winter. Comparing *Slope* in the urban and rural areas, there was a decreasing tendency of SUHI in summer daytime and winter nighttime, with increasing tendency in winter daytime and summer nighttime. The characteristics of urban thermal environment in Type D cities were quite different from other types (Zhou et al., 2016), and the specific reasons for these phenomena remained to be clarified. As Fan et al. (2017) noticed the impact of urban size might be a possible influencing factor.

In general, the summer nighttime was the key temporal period for urban thermal environment management. According to previous studies, the nighttime SUHI manifested the urbanization induced local

Table 2
Mean *Slope* (°C/year) in winter, summer, daytime and nighttime of urban and rural areas within each city type.

Cities		Summer daytime		Summer nighttime		Winter daytime		Winter nighttime	
City type	Number of cities	Urban	Rural	Urban	Rural	Urban	Rural	Urban	Rural
A	75	0.01	0.04	0.02	0.00	0.36[a]	0.40[a]	0.30[a]	0.27[a]
B	133	−0.04	−0.04	0.02	0.00	0.07	0.11[a]	0.13[a]	0.10[a]
C	45	0.24[a]	0.27[a]	0.11[a]	0.08	−0.11[a]	−0.08	0.03	0.02
D	32	0.01	0.03	0.05	0.02	−0.36[a]	−0.38[a]	−0.26[a]	−0.26[a]

All slopes are statistically significant ($P < 0.05$).
[a] $|Slope| \geq 0.10$.

climate change due to the unequal diurnal surface energy budget, i.e. urban heat absorption and release in the day time and nighttime respectively (Clinton and Gong, 2013; Peng et al., 2012; Voogt and Oke, 2003). This would be further intensified in the process of urbanization with the increasing heat emission from urban transportation and industry, as well as the enlarged heat absorption resulted from artificial surface expansion (W. Zhou et al., 2014). Consequently, the mitigation and adaptation strategies of urban thermal environment management should be focused on reducing the nighttime SUHI effect in the vital zone cities, as well as in the major zone cities. For SUHI alleviation, green infrastructures, rooftop gardens, optimization of building materials (Asgarian et al., 2015; Norton et al., 2015; Yu et al., 2017) and other urban renewal approaches (Elmes et al., 2017; Li et al., 2011; Xie et al., 2013) had been proved to be effective, together with controlling the sources of anthropogenic heat, such as vehicle exhaust (Mohajerani et al., 2017).

4. Conclusions

The understanding of variation of surface thermal environment is essential for SUHI adaptation and mitigation. In this study, the urban and rural areas of 285 cities in China were identified based on land use data. Then, the spatial-temporal change characteristics of surface thermal environment were analyzed from the contrast perspective of urban and rural areas, summer and winter, and daytime and nighttime. The results showed that, 98.9% cities exhibited SUHI effect in summer nighttime, with the stronger SUHI in northern cities compared with that in southern cities, which was invariant with the seasons. Focusing on the differences of the mean SUHI, it could be found that in summer daytime, the mean SUHI was the largest, and 4.6% of the cities experienced an extreme SUHI over 4 °C. Through analyzing spatial patterns of LST change, the warming areas in winter were more intensively located in southeastern China, compared with the distribution in arid and semi-arid areas of northern China in summer. Furthermore, in summer nighttime, there were more cities having higher *Slope* in urban areas than in rural areas, indicating the importance of summer nighttime for SUHI adaptation. All the cities were classified into four types based on LST change trend, with type A and B cities identified as the vital zone and major zone of SUHI adaptation, respectively.

To enhance the ability of cities to adapt to climate change and provide more effective approaches for mitigating SUHI effects, future research should be conducted to explore the driving factors of SUHI in summer nighttime and their regional differences. Meanwhile, the seasonal SUHI and the local climate influence on thermal environment need to be considered. Thus, it is expected to gain more practical guidance to the prevention of the ecological risk in the process of China's new urbanization.

Acknowledgments

This research was financially supported by the National Natural Science Foundation of China (41671182) and the 111 Project (B14001).

References

Asgarian, A., Amiri, B.J., Sakieh, Y., 2015. Assessing the effect of green cover spatial patterns on urban land surface temperature using landscape metrics approach. Urban. Ecosyst. 18, 209–222.
Benz, S.A., Bayer, P., Blum, P., 2017. Identifying anthropogenic anomalies in air, surface and groundwater temperatures in Germany. Sci. Total Environ. 584–585, 145–153.
Chapman, S., Watson, J.E.M., Salazar, A., Thatcher, M., Mcalpine, C.A., 2017. The impact of urbanization and climate change on urban temperatures: a systematic review. Landsc. Ecol. 32, 1921–1935.
Chen, J., Ban, Y., Li, S., 2014. China: open access to earth land-cover map. Nature 514, 434.
Chen, Y., Liu, X., Li, X., Liu, X., Yao, Y., Hu, G., Xu, X., Pei, F., 2017. Delineating urban functional areas with building-level social media data: a dynamic time warping (DTW) distance based K-medoids method. Landsc. Urban Plan. 160, 48–60.
Clinton, N., Gong, P., 2013. MODIS detected surface urban heat islands and sinks: global locations and controls. Remote Sens. Environ. 134, 294–304.
Dan, S.M., Dan, B., Xu, H.X., Xue, W.R., Xia, J., 2011. Analysis of impact of urban development on heat island effect in Chengdu city. Environ. Sci. Technol. 34, 180–185.
Du, H., Wang, D., Wang, Y., Zhao, X., Qin, F., Jiang, H., Cai, Y., 2016. Influences of land cover types, meteorological conditions, anthropogenic heat and urban area on surface urban heat island in the Yangtze River Delta urban agglomeration. Sci. Total Environ. 571, 461–470.
Elmes, A., Rogan, J., Williams, C., Ratick, S., Nowak, D., Martin, D., 2017. Effects of urban tree canopy loss on land surface temperature magnitude and timing. ISPRS J. Photogramm. Remote Sens. 128, 338–353.
Fan, C., Myint, S.W., Kaplan, S., Middel, A., Zheng, B., Rahman, A., Huang, H., Brazel, A., Blumberg, D.G., 2017. Understanding the impact of urbanization on surface urban heat islands—a longitudinal analysis of the oasis effect in subtropical desert cities. Remote Sens. 9:672. https://doi.org/10.3390/rs9070672.
Gunawardena, K.R., Wells, M.J., Kershaw, T., 2017. Utilising green and bluespace to mitigate urban heat island intensity. Sci. Total Environ. 584–585, 1040–1055.
Hu, L., Brunsell, N.A., 2013. The impact of temporal aggregation of land surface temperature data for surface urban heat island (SUHI) monitoring. Remote Sens. Environ. 134, 162–174.
Imhoff, M.L., Zhang, P., Wolfe, R.E., Bounoua, L., 2010. Remote sensing of the urban heat island effect across biomes in the continental USA. Remote Sens. Environ. 114, 504–513.
Kuang, W., Liu, Y., Dou, Y., Chi, W., Chen, G., Gao, C., Yang, T., Liu, J., Zhang, R., 2015. What are hot and what are not in an urban landscape: quantifying and explaining the land surface temperature pattern in Beijing, China. Landsc. Ecol. 30, 357–373.
Kuang, W., Liu, J., Dong, J., Chi, W., Zhang, C., 2016. The rapid and massive urban and industrial land expansions in China between 1990 and 2010: a CLUD-based analysis of their trajectories, patterns, and drivers. Landsc. Urban Plan. 145, 21–33.
Li, J., Song, C., Cao, L., Zhu, F., Meng, X., Wu, J., 2011. Impacts of landscape structure on surface urban heat islands: a case study of Shanghai, China. Remote Sens. Environ. 115, 3249–3263.
Li, X., Zhou, Y., Asrar, G.R., Imhoff, M.L., Li, X., 2017. The surface urban heat island response to urban expansion: a panel analysis for the conterminous United States. Sci. Total Environ. 605–606, 426–435.
Liu, J., Kuang, W., Zhang, Z., Xu, X., Qin, Y., Ning, J., Zhou, W., Zhang, S., Li, R., Yan, C., Wu, S., Shi, X., Jiang, N., Yu, D., Pan, X., Chi, W., 2014. Spatiotemporal characteristics, patterns, and causes of land-use changes in China since the late 1980s. J. Geogr. Sci. 24, 195–210.
Liu, Y., Fang, X., Xu, Y., Zhang, S., Luan, Q., 2017. Assessment of surface urban heat island across China's three main urban agglomerations. Theor. Appl. Climatol. https://doi.org/10.1007/s00704-017-2197-3.
Mariani, L., Parisi, S.G., Cola, G., Lafortezza, R., Colangelo, G., Sanesi, G., 2016. Climatological analysis of the mitigating effect of vegetation on the urban heat island of Milan, Italy. Sci. Total Environ. 569–570, 762–773.
Merte, S., 2017. Estimating heat wave-related mortality in Europe using singular spectrum analysis. Clim. Chang. 142, 321–330.
Mohajerani, A., Bakaric, J., Jeffreybailey, T., 2017. The urban heat island effect, its causes, and mitigation, with reference to the thermal properties of asphalt concrete. J. Environ. Manag. 197, 522–538.
Nishiyama, K., Endo, S., Jinno, K., Uvo, C.B., Olsson, J., Berndtsson, R., 2007. Identification of typical synoptic patterns causing heavy rainfall in the rainy season in Japan by a self-organizing map. Atmos. Res. 83, 185–200.
Norton, B.A., Coutts, A.M., Livesley, S.J., Harris, R.J., Hunter, A.M., Williams, N.S.G., 2015. Planning for cooler cities: a framework to prioritise green infrastructure to mitigate high temperatures in urban landscapes. Landsc. Urban Plan. 134, 127–138.
Peng, S., Piao, S., Ciais, P., Friedlingstein, P., Ottle, C., Bréon, F.M., Nan, H., Zhou, L., Myneni, R.B., 2012. Surface urban heat island across 419 global big cities. Environ. Sci. Technol. 46, 696–703.
Peng, J., Xie, P., Liu, Y., Ma, J., 2016. Urban thermal environment dynamics and associated landscape pattern factors: a case study in the Beijing metropolitan region. Remote Sens. Environ. 173, 145–155.
Rizwan, A.M., Dennis, L.Y.C., Liu, C., 2008. A review on the generation, determination and mitigation of Urban Heat Island. J. Environ. Sci. (China) 20, 120–128.
Rozenfeld, H.D., Rybski, D., Andrade, J.S., Batty, M., Stanley, H.E., Makse, H.A., 2008. Laws of population growth. Proc. Natl. Acad. Sci. U. S. A. 105, 18702–18707.
Schwarz, N., Lautenbach, S., Seppelt, R., 2011. Exploring indicators for quantifying surface urban heat islands of European cities with MODIS land surface temperatures. Remote Sens. Environ. 115, 3175–3186.
Seto, K.C., Fragkias, M., Güneralp, B., Reilly, M.K., 2011. A meta-analysis of global urban land expansion. PLoS One https://doi.org/10.1371/journal.pone.0023777.
Seto, K.C., Güneralp, B., Hutyra, L.R., 2012. Global forecasts of urban expansion to 2030 and direct impacts on biodiversity and carbon pools. Proc. Natl. Acad. Sci. U. S. A. 109, 16083–16088.
Shen, H., Huang, L., Zhang, L., Wu, P., Zeng, C., 2016. Long-term and fine-scale satellite monitoring of the urban heat island effect by the fusion of multi-temporal and multi-sensor remote sensed data: a 26-year case study of the city of Wuhan in China. Remote Sens. Environ. 172, 109–125.
Shi, B., Tang, C.S., Gao, L., Liu, C., Wang, B.J., 2012. Observation and analysis of the urban heat island effect on soil in Nanjing, China. Environ. Earth Sci. 67, 215–229.
Shiflett, S.A., Liang, L.L., Crum, S.M., Feyisa, G.L., Wang, J., Jenerette, G.D., 2017. Variation in the urban vegetation, surface temperature, air temperature nexus. Sci. Total Environ. 579, 495–505.
Song, W., Deng, X., 2015. Effects of urbanization-induced cultivated land loss on ecosystem services in the North China Plain. Energies 8, 5678–5693.
Song, J., Du, S., Feng, X., Guo, L., 2014. The relationships between landscape compositions and land surface temperature: quantifying their resolution sensitivity with spatial regression models. Landsc. Urban Plan. 123, 145–157.

Tran, D.X., Pla, F., Latorre-Carmona, P., Myint, S.W., Caetano, M., Kieu, H.V., 2017. Characterizing the relationship between land use land cover change and land surface temperature. ISPRS J. Photogramm. Remote Sens. 124, 119–132.
Voogt, J.A., Oke, T.R., 2003. Thermal remote sensing of urban climates. Remote Sens. Environ. 86, 370–384.
Walelign, S.Z., 2016. Livelihood strategies, environmental dependency and rural poverty: the case of two villages in rural Mozambique. Environ. Dev. Sustain. 18, 593–613.
Wang, X., Sun, X., Tang, J., Yang, X., 2015. Urbanization-induced regional warming in Yangtze River Delta: potential role of anthropogenic heat release. Int. J. Climatol. 35, 4417–4430.
Wang, J., Huang, B., Fu, D., Atkinson, P.M., Zhang, X., 2016. Response of urban heat island to future urban expansion over the Beijing–Tianjin–Hebei metropolitan area. Appl. Geogr. 70, 26–36.
Weng, Q., Lu, D., Schubring, J., 2004. Estimation of land surface temperature–vegetation abundance relationship for urban heat island studies. Remote Sens. Environ. 89, 467–483.
Xie, M., Wang, Y., Chang, Q., Fu, M., Ye, M., 2013. Assessment of landscape patterns affecting land surface temperature in different biophysical gradients in Shenzhen, China. Urban. Ecosyst. 16, 871–886.
Yang, C., He, X., Yan, F., Yu, L., Bu, K., Yang, J., Chang, L., Zhang, S., 2017. Mapping the influence of land use/land cover changes on the urban heat island effect—a case study of Changchun, China. Sustainability 9:312. https://doi.org/10.3390/su9020312.
Yao, R., Luo, Q., Luo, Z., Jiang, L., Yang, Y., 2015. An integrated study of urban microclimates in Chongqing, China: historical weather data, transverse measurement and numerical simulation. Sustain Cities Soc. 14, 187–199.
Yao, R., Wang, L., Huang, X., Niu, Z., Liu, F., Wang, Q., 2017. Temporal trends of surface urban heat islands and associated determinants in major Chinese cities. Sci. Total Environ. 609, 742–754.
Yu, Z., Guo, X., Jørgensen, G., Vejre, H., 2017. How can urban green spaces be planned for climate adaption in subtropical cities? Ecol. Indic. 82, 152–162.
Yu, Z., Guo, X., Zeng, Y., Koga, M., Vejre, H., 2018. Variations in land surface temperature and cooling efficiency of green space in rapid urbanization: the case of Fuzhou city, China. Urban For. Urban Green. 29, 113–121.
Zhang, P., Imhoff, M.L., Wolfe, R.E., Bounoua, L., 2010. Characterizing urban heat islands of global settlements using MODIS and nighttime lights products. Can. J. Remote. Sens. 36, 185–196.
Zhao, L., Lee, X., Smith, R.B., Oleson, K., 2014. Strong contributions of local background climate to urban heat islands. Nature 511, 216–219.
Zhou, L., Dickinson, R.E., Tian, Y., Fang, J., Li, Q., Kaufmann, R.K., Tucker, C.J., Myneni, R.B., 2004. Evidence for a significant urbanization effect on climate in China. Proc. Natl. Acad. Sci. U. S. A. 101, 9540–9544.
Zhou, W., Qian, Y., Li, X., Li, W., Han, L., 2014. Relationships between land cover and the surface urban heat island: seasonal variability and effects of spatial and thematic resolution of land cover data on predicting land surface temperatures. Landsc. Ecol. 29, 153–167.
Zhou, D., Zhao, S., Liu, S., Zhang, L., Zhu, C., 2014. Surface urban heat island in China's 32 major cities: spatial patterns and drivers. Remote Sens. Environ. 152, 51–61.
Zhou, D., Zhang, L., Hao, L., Sun, G., Liu, Y., Zhu, C., 2016. Spatiotemporal trends of urban heat island effect along the urban development intensity gradient in China. Sci. Total Environ. 544, 617–626.
Zhou, W., Pickett, S.T.A., Cadenasso, M.L., 2017a. Shifting concepts of urban spatial heterogeneity and their implications for sustainability. Landsc. Ecol. 32, 15–30.
Zhou, W., Wang, J., Cadenasso, M.L., 2017b. Effect of the spatial configuration of trees on urban heat mitigation: a comparative study. Remote Sens. Environ. 195, 1–12.